Heliyon 10 (2024) e38958

Contents lists available at ScienceDirect

Heliyon

journal homepage: www.cell.com/heliyon

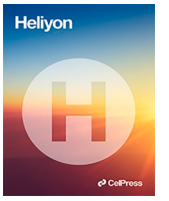

Research article

Tile: Construction of a specific nanoprobe for scavenging ROS in hypobaric hypoxia induced brain injury of mice

Xiaobo Wang [a], Fuhan Fan [b], Ya Hou [c,*], Xianli Meng [a,b,c,**]

[a] *Innovative Institute of Chinese Medicine and Pharmacy/Academy for Interdiscipline, Chengdu University of Traditional Chinese Medicine, Chengdu, 611137, China*
[b] *School of Pharmacy/School of Modern Chinese Medicine Industry, Chengdu University of Traditional Chinese Medicine, Chengdu, 611137, China*
[c] *TCM Regulating Metabolic Diseases Key Laboratory of Sichuan Province, Hospital of Chengdu University of Traditional Chinese Medicine, Chengdu, 610075, Sichuan, China*

ARTICLE INFO

Keywords:
RuPc-BSA
Hypobaric hypoxia brain injury
ROS scavenger
Keap1/Nrf2 signaling pathway

ABSTRACT

The prevention and treatment of hypobaric hypoxia brain injury (HHBI) remains an unprecedented challenge due to the complex oxidative stress response at the damage site. In this study, RuCO phthalocyanine compound (RuPc) and bovine serum albumin (BSA) were self-assembled to obtain RuPc-BSA nanoparticles for HHBI therapy. As a nanoprobe carrying and storing carbon monoxide (CO), RuPc-BSA delivers CO to pathologically damaged areas of the brain. CO specifically attaches itself to the heme functional groups on mitochondria and restricts the source of reactive oxygen species (ROS) generation. RuPc-BSA nanoparticles have been demonstrated *in vitro* to exhibit amazing stability as well as remarkable scavenging activity on hydroxyl radical, superoxide anion, and hydrogen peroxide. *In vivo* experiments showed that ROS levels in the brain of HHBI rats pretreated with RuPc-BSA decreased significantly, and neuronal function and oxidative stress levels were alleviated. Western blot and qRT-RCR results indicated that RuPc-BSA restricted the protein levels of Keap1, whereas enhanced the gene and protein levels of Nrf2. This study demonstrated that RuPc-BSA can ameliorate HHBI of mice by scavenging ROS partly via activating Keap1/Nrf2 signaling pathway.

1. Introduction

Plateaus and high-altitude regions account for a substantial proportion of the earth, being the most challenging environments for human survival [1]. It has been confirmed that hypobaric hypoxia (HH) at a high-altitude environment can cause hypobaric hypoxia brain injury (HHBI) [2–4], such as acute mountain sickness (AMS), high altitude cerebral edema, and cerebral hemorrhage, a series of brain injury symptoms or disease associated with brain dysfunction [5–7]. Prior research has indicated that oxidative stress, inflammatory response, mitochondrial dysfunction, and disruption of the blood-brain barrier (BBB) are the primary pathogenic processes associated with HHBI [8–10]. Reactive oxygen species (ROS) consume antioxidant molecules such as glutathione peroxidase (GSSH-PX), catalase (CAT), and superoxide dismutase (SOD) to create a homeostatic tilt between ROS and the antioxidant system after

* Corresponding author.
** Corresponding author. Innovative Institute of Chinese Medicine and Pharmacy/Academy for Interdiscipline, Chengdu University of Traditional Chinese Medicine, Chengdu, 611137, China.
E-mail addresses: yahou@cdutcm.edu.cn (Y. Hou), xlm999@cdutcm.edu.cn (X. Meng).

https://doi.org/10.1016/j.heliyon.2024.e38958
Received 30 October 2023; Received in revised form 28 September 2024; Accepted 3 October 2024
Available online 4 October 2024

HH exposure [11]. Overproduction of ROS will directly alter or break down cellular macromolecules including membranes, proteins, lipids, and DNA, triggering subsequent inflammatory reactions and the release of protease secretion [12,13]. These products eventually cause brain damage through a variety of intricate interactions, including necrosis, apoptosis, inflammation, and autophagy. Nowadays, the most common medications used to treat HHBI are hormone replacement therapy and neuroprotective medications such edaravone and dexamethasone [14–16]. The use of this class of medicines is limited despite their ability to quickly cure hypoxic symptoms due to the unavoidable targeting issues and the danger of cardiovascular and cerebrovascular harm [17]. One potential approach to treat and prevent HHBI at altitude environment may target removal of ROS from the brain to interdict the oxidative stress injury of nerve cells.

Carbon monoxide (CO) offers a potential therapeutic approach for HHBI as a novel way to reduce oxidative stress damage by ROS focused clearance [18]. It has been reported that consuming too much of CO can decrease hemoglobin's ability to carry and release oxygen, and lead to mitochondrial damage [16,19,20]. Nonetheless, several earlier investigations have demonstrated that both endogenous and exogenous CO can control vascular function, oxidative stress, apoptosis, and proliferation through a range of signaling pathways at healthy doses [21,22]. As the main site of ROS production in cells, the ROS content of mitochondria surges under hypoxic conditions, which will eventually lead to mitochondrial malfunction [23,24]. It has been found that CO can selectively bind the functional groups of mitochondrial cytochrome heme, impairing mitochondrial function and reducing the generation of ROS [20,25]. Simultaneously, CO has been shown to inhibit nicotinamide adenine dinucleotide phosphate (NADPH) oxidase activity, which in turn lowers the generation of superoxide anions (O_2^-, a subclass of ROS molecules) [26]. Because of CO's limited water solubility, it was challenging to guarantee that CO is delivered to the target tissue in its original form. Therefore, how to release CO in target organs is the first obstacle of limiting its clinical treatment for HHBI [27]. Promisingly, Motterlini and his colleagues proposed that a transition metal carbonyl complex can be viewed as a carbon monoxide releasing molecules (CORMS) or CO carrier to transport CO to tissue regions of interest in a safe, stable and measurable way [28]. After that, numerous metal carbonyl complexes and related complexes

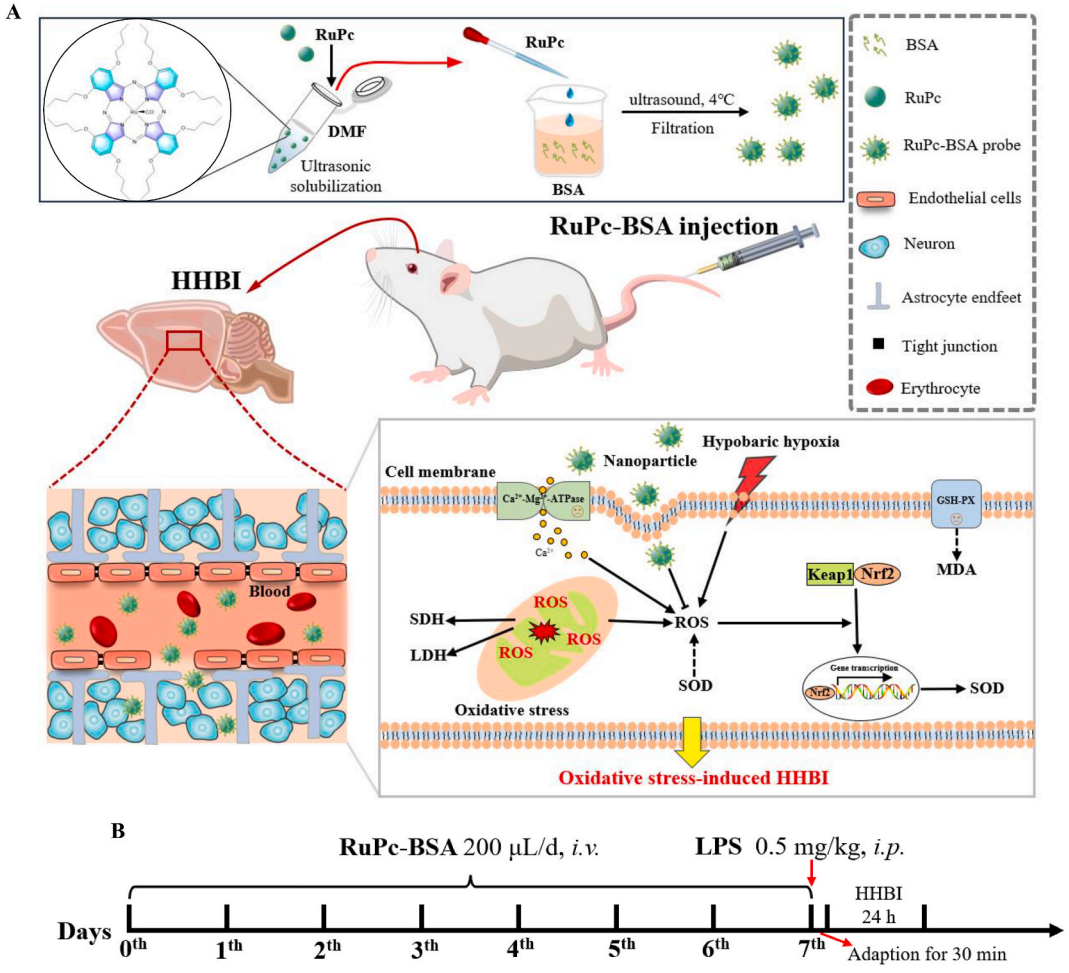

Fig. 1. The synthesis process of RuPc-BSA and the mechanism of alleviating HHBI. (A) The synthesis principle of RuPc-BSA and its schematic diagram alleviating oxidative stress damage in HHBI mice by targeting CO release, reducing ROS production and activating Nrf2/Keap1 signaling pathway. (B) Construction process of HHBI mouse model and treatment by RuPc-BSA.

have been designed and synthesized, exerting remarkable practicality and applicability in corresponding animal and cell disease models by releasing a specific concentration of CO in the injured tissue or organelle. 1, 4, 8, 11, 15, 18, 22, 25 – octabutoxy - 29H, 31H - Ruthenium (II) phthalocyanine (RuCO phthalocyanine compound, RuPc) is a CO releasing molecule with CORMs structure, which has great potential for the treatment of oxidative stress damage caused by altitude hypoxia stimulation [29,30].

In this work, we plan to couple RuPc with bovine serum albumin (BSA) to construct a novel CORMS (RuPc-BSA) with higher water solubility and biosafety. And we aim to investigate its potential to cure HHBI of mice by consuming excessive ROS and the underlying molecular mechanism of inhibiting oxidative stress injury.

2. Materials and methods

2.1. Reagents and chemicals

Phosphate buffered saline (PBS, C10010500) was acquired by Gibco ThermoFisher Scientific (Waltham, USA). N, N-dimethylformamide (DMF, R004209) weas provided by Shanghai Yien Chemical Technology Co., Ltd. (Shanghai, China). Lipopolysaccharide (0000114326) was purchased from Sigma-Aldrich (Saint Louis, USA). DCFH-DA detection kit (E004-1-1), LDH (A020-2), SOD (A001-3), MDA (A003-1), CAT (A007-1-1), GSSG (A061-1), and GSH-PX (A005-1) were provided by Jiancheng Bioengineering Institute Co., Ltd. (Nanjing, China). Total RNA isolation kit (R211001) was obtained from Foregene Co., Ltd. (Chengdu, China). Primary antibodies against Nrf2 (A3577) and Keap1 (A17062) were supplied by ABclonal Technology Co., Ltd. (Wuhan, China). 4 % paraformaldehyde (BL539A) was procured from Labgic Technology Co., Ltd. (Beijing, China). Blood cytometer flush soluti on (V-28R), hemolytic agent (V-28CFL), diluent (V-28D), and E-Z cleaning solution (V-28E) were purchased from Mindray Bio-Medical Electronics Co., Ltd. (Shenzhen, China).

2.2. Animals

20 ± 2 g male BALB/c mice (6–8 weeks) were purchased from Hunan SJA Laboratory Animal Co., Ltd. (License Number: SCXK (Xiang) 2019-004). Following quarantine, the mice were fed with conventional diet at a temperature of 23 ± 2 °C and a humidity of 60 ± 5 %, with a 12 h cycle of darkness and light (License Number: SYXK (Chuan) 2020-124).

2.3. Preparation of RuPc-BSA

RuPc-BSA was synthesized according to the principle of Fig. 1 A. In brief, 3 mg RuPc was dissolved in 0.5 mL DMF. And after being ultrasonic for 3 h until complete dissolution, the RuPc suspension was then added drop by drop to 4 mL deionized water containing 40 mg BSA to acquire RuPc-BSA. Ultrasound was performed in the ice bath for 5 min and then centrifugally filtered using an Amicon filter to remove excess unbound RuPc. At the last, RuPc-BSA nanoprobes were collected after centrifuging at 2000 rpm for 10 min.

2.4. Characterization

As previously reported, the morphology of RuPc-BSA particles was observed by scanning electron microscope (SEM, Hitachi S-4800, Hitachi, JPN). Dynamic light scattering technique (NANO-S90, Malvern Instruments, UK) and Zetasizer Nano Series (Malvern Instruments, UK) were adopted to determine the hydrodynamic diameter and zeta potential of RuPc-BSA in distilled water containing 10 % fetal bovine serum. The combination degree and nanomaterials loading efficiency of RuPc and BSA were measured by Ultraviolet–visible spectrophotometer (Beckman Coulter DU 730, UV Spectrophotometer).

2.5. Stability

In order to characterize the stability of RuPc and BSA binding, the hydrated particle size changes of RuPc-BSA nanoparticles in different solvents were detected. To configure nanoparticle solutions of equal concentration, RuPc-BSA was dissolved in water, PBS, hydrogen peroxide (H_2O_2) solution, and complete medium. Then, variations in the hydrated particle size in various solvents were used to evaluate the stability of RuPc-BSA for five days in a row.

2.6. In vitro ROS scavenging capacity of RuPc-BSA

To characterize the ROS scavenging potential of RuPc-BSA, we examined the scavenging capacity of RuPc-BSA against hydroxyl radical ($HO^{\bullet}$), H_2O_2 and O_2^- *in vitro*. In brief, add RuPc-BSA and the appropriate detection reagent after setting up the control and measurement group as per the instructions. Following incubation, the absorbance value of the samples at the appropriate wavelength was determined using UV–VIS spectroscopy (Beckman Coulter DU 730, UV Spectrophotometer).

2.7. Establishment of HHBI model

Thirty Balb/c mice were randomized into three groups: control group (saline), model group (saline), and RuPc-BSA nanoparticle group (200 μL, intravenous injection for 7 consecutive days). Except for the control group, each mouse received an intraperitoneal

injection of 0.5 mg/kg lipopolysaccharide after the final treatment. Then, following our previous modeling method [31], the mice were quickly transferred to a sealed low-pressure oxygen chamber for a 30 min environmental acclimatization (Fig. 1 B). The low-pressure oxygen chamber was then unlocked, and the specifications were set so that it rose to 7000 m at a constant speed of 50 m/s. After 24 h of hypobaric hypoxic stimulation, mice were transferred to atmospheric pressure environment to collect the brain tissue and blood sample. Blood was centrifuged at 4 °C for 10 min at 3500 rpm in order to acquire serum samples. After being rinsed with pre-cooled saline, the removed brain tissue was split into the left and right hemispheres and kept at 4 % paraformaldehyde or −80 °C, respectively.

2.8. Hematoxylin-eosin (H&E) staining

According to reported research [32], the pathological changes of HHBI were assessed using H&E staining. Gradient alcohol was used to dehydrate mouse brain tissues fixed with 4 % paraformaldehyde, and paraffin was used for standard embedding. Brain tissue was then cut into coronal sections with a thickness of 5 μm using a microtome (TP1020, Leica). According to the instructions of the kit, sections were deparaffinized, rehydrated and stained. After that, it was translucent with xylene, dehydrated with gradient alcohol, and sealed with resin glue. Finally, the pathological damage to the cortex and hippocampus of the brain was observed using a Leica microimaging equipment (DM6B, Leica).

2.9. Nissl staining

As we previously reported [33], Nissl staining was used to evaluate changes in neuronal vitality. According to the kit instructions, 5 μm paraffin coronal sections of brain tissue was deparaffinized and rehydrated using xylene and gradient alcohol before being stained with 0.1 % toluidine blue to identify neuronal Nissl bodies. Finally, a microscopic imaging system and light microscopy (DM6B, Leica) were used to monitor and measure global morphological changes and neuronal activity.

2.10. Detection of ROS

Freshly isolated mouse brain tissue was immediately sliced into minute pieces with ophthalmic scissors after being cleaned with precooled PBS. After being enzymatically digested for 20 min at 37 °C in a water bath, the cells were extracted from the tissues and collected by filtering through nylon mesh. Following a 10-min centrifugation at 2000 rpm, the cell precipitate was washed twice with PBS. According to the instructions of DCFH-DA kit, cell samples were separated into negative control, positive control, and sample tubes before being incubated with DCFH-DA probe diluent at 37 °C for 30 min. Centrifugation was used to separate the cell precipitates for 5 min at 1000 rpm, followed by washed twice with PBS. Finally, the treated cell samples were resuspended with PBS, and flow cytometry system (FACSCanto II, BD Biosciences) was used to measure the fluorescence signals of the cells at the excitation/emission wavelength of 488/525 nm.

2.11. Determination of LDH, SOD, MDA, CAT, GSSG and GSH-PX activities

According to the previously reported study [34], LDH, SOD, MDA, CAT, GSSG, and GSH-PX activities were detected. In brief, brain tissue homogenates from HHBI mice were treated, and centrifuged at 5000 rpm for 15 min to extract the supernatants. The protein concentration of tissue samples was determined using the BCA kit according to the experimental method provided by the kit. Next, according to the operating steps in the instruction manual, blank wells, standard wells, measurement wells and control wells were set up, and the respective test samples and working solutions were added to the cell detection plate. Cells were then incubated at the temperatures and times specified in the kit instructions. Finally, the absorbance value at the corresponding wavelength was measured.

2.12. Immunofluorescence assay

Immunofluorescence staining was performed according to previous reports [9]. In simple terms, after dewaxing the sections with xylene and gradient ethanol, the antigens were repaired with EDTA antigen repair buffer. After being blocked with 5 % BSA for 30 min, the slices were incubated with primary antibodies against Keap1 and Nrf2 at 4 °C overnight with a dilution ratio of 1:100. The next day, slices were incubated with goat anti-rabbit IgG antibody coupled with cy3 at 37 °C for 1 h, and the nucleus was stained with DAPI. At the same time, images were captured using a fluorescence microscope (NIKON ECLIPSE C1, NIKON Corporation, Tokyo, Japan). Immunoreactivity density was analyzed using Image-Pro Plus 6.0 software (Media cybernetics, Inc., Rockville, MD).

2.13. Quantitative real-time PCR (qRT-PCR)

Total RNA was extracted from brain tissue of HHBI mice according to the instructions of Foregene total RNA isolation kit. The first strand template cDNA was synthesized by reverse transcription. Nrf2 and Keap1 mRNA expression level was detected by qRT - PCR using PCR amplification of premix with appropriate dilution of cDNA solution and corresponding primers. β-actin was used as an internal reference gene. The thermocycling conditions were set as follows: Initial denaturation at 95 °C for 30 s, followed by 40 cycles comprising of denaturation at 95 °C for 5 s; Annealing at 60 °C for 30 s; Elongation at 72 °C for 30 s; And extension at 72 °C for 5 min. The primer sequences used were as follows: Nrf2, forward: 5′- ACATGGAGCAAGTTTGGCAG-3′, reverse: 5′-TGGA-GAGGATGCTGCTGAAA-3’; Keap1, forward: 5′-AGCGTGGAGAGAGATATGAGCC-3′, reverse: 5′- ATCATCCGCCACTCATTCCT-3’;

β-actin, forward: 5′- TGAGAGGGAAATCGTGCGTGAC-3′, reverse: 5′- GCTCGTTGCCAATAGTGATGACC-3’. The target genes expression levels were calculated as $2^{-\Delta\Delta Cq}$ ($\Delta\Delta Cq = Cq_{target}\text{-}C\ q_{\beta\text{-}actin}$)

2.14. Western blot analysis

RIPA solution containing protease and phosphatase inhibitors was used to thaw and homogenize mouse brain tissue. Following a 10-min centrifugation at 10,000 rpm at 4 °C, the protein content on the supernatant samples was ascertained using a BCA protein detection kit. Western blot is performed according to the steps described in our previous study [15]. In short, the target proteins were isolated by 10 % SDS-PAGE and transferred to a 0.45 μm-PVDF membrane. The membrane was then blocked with 5 % BSA at room temperature for 1.5 h and was incubated with Nrf2 (1:1000), Keap1 (1:1000) and β-actin (1:1000) at 4 °C overnight. The next day, bands were washed 3 times with TBST and incubated with goat anti-rabbit immunoglobulin G (1:10,000 diluent) labeled with horseradish peroxidase at room temperature for 2 h. The bands were then visualized using an enhanced chemiluminescent reagent solution and the images were captured using the Visionworks imaging system (UVP iBox Scientia, Germany).

2.15. Hemolysis test

Blood from healthy BALB/c mice was collected and placed in an anticoagulant tube containing EDTA-K2. And blood cells were extracted and acquired by centrifuging at 3500 rpm at 4 °C for 15 min. Different volumes of RuPc-BSA were dissolved in PBS to prepare RuPC-BSA gradient solutions with concentrations of 0, 10, 25, 50, and 100 μg/mL 20 μL blood cells were mixed with 1 mL RuPc-BSA gradient solution and ddH_2O, and incubated at 37 °C for 1 h. The sample was centrifuged at 3000 rpm at 4 °C for 15 min, and the sample was placed at the same level to record the hemolysis. 200 μL supernatant of the sample was added into the 96-well plate, and the absorbance of 542 nm was detected using a microhole reader (Flexstation3, Molecular Devices).

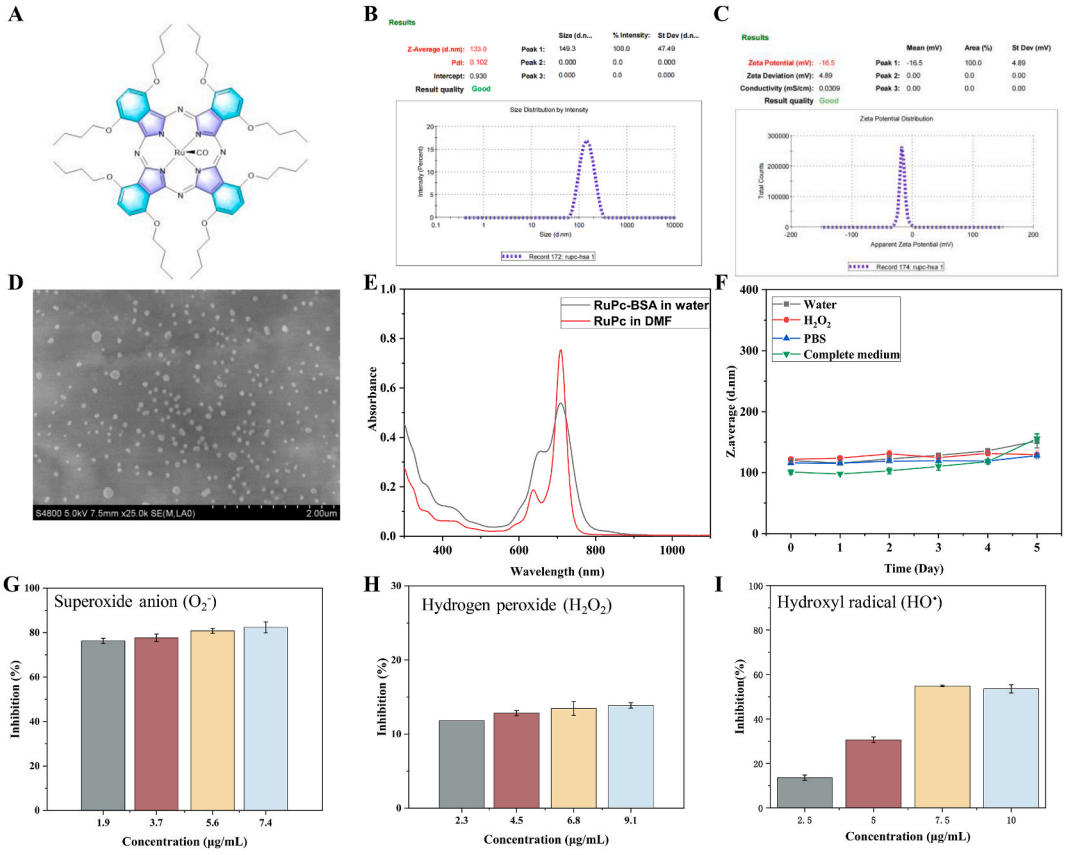

Fig. 2. Physicochemical characterization of RuPc-BSA and *in vitro* ROS-responsive release. (A) Chemical structure of RuPc. (B, C) Hydration size, polydispersion coefficient and zeta potential of RuPc-BSA nanoparticle. (D) Representative SEM image of RuPc-BSA. (E) Ultraviolet absorption spectrum. (F) Stability test results of RuPc-BSA nanoparticles in different solvents. (G, H and I) The scavenging effect of RuPc-BSA nanoparticles with different concentration on O_2^-, H_2O_2 and HO•.

2.16. Biosafety assessment

To explore the potential side effects of the RuPc-BSA nanoparticle, healthy male BALB/c mice were given 200 μL of RuPc-BSA solution and PBS intravenously for 7 days. After the last dose and a 24 h interval, the whole blood of mice was collected for blood routine testing. At the same time, the heart, liver, spleen, lung, kidney and brain tissues of mice were harvested, and the toxic and side effects of nanoprobe RuPc-BSA were analyzed by H&E staining.

2.17. Statistical analysis

Data analyses were performed using GraphPad Prism 9.0 by one-way analysis of variance followed by a Tukey's multiple comparisons test. Data were expressed as mean ± standard deviation from at least three independent experiments. $p < 0.05$ was deemed statistically significant.

3. Results

3.1. Characterization of RuPc-BSA

The structure of RuPc is shown in Fig. 2 A, and the particle size, polydispersity index and zeta potential were measured to verify the physical and chemical properties of the nanoparticles. As shown in Fig. 2 B, the hydrated particle size of RuPc-BSA is 133 nm, and the

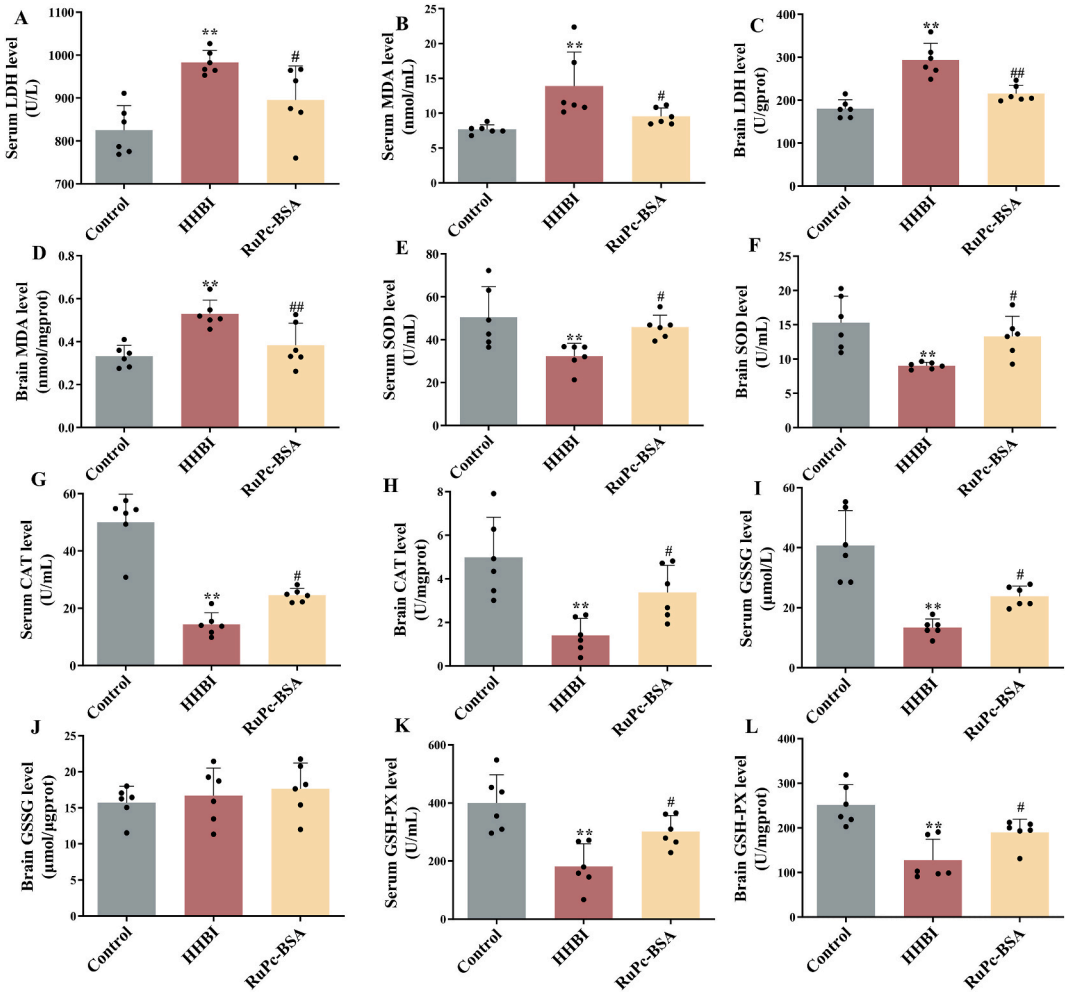

Fig. 3. RuPc-BSA reduces oxidative stress damage in HHBI mice. The levels of LDH (A) and MDA (B) in serum, and the LDH (C) and MDA (D) levels in brain tissue. Effect of RuPc-BSA on SOD levels (E, serum; F, brain tissue), CAT levels (G, serum; H, brain tissue), GSSG levels (I, serum; J, brain tissue) and GSH-PX levels (K, serum; L, brain tissue) of HHBI mice. Data above were presented as mean ± SD, n = 6. *$p < 0.05$ and **$p < 0.01$ vs the control group; $^{\#}p < 0.05$ and $^{\#\#}p < 0.01$ vs the HHBI group.

fitting curve is regular and conforms to the shape of Gaussian curve. The PDI and charge values of RuPc-BSA are 0.102 and −16.5 mv, respectively, indicating that the nanoparticle system is stable and relatively uniform (Fig. 2C). The morphology of RuPc-BSA was then observed by scanning electron microscopy, and it was found that it was spherical and relatively evenly dispersed in solvent (Fig. 2 D). At the same time, Ultraviolet–visible spectroscopy revealed that absorption spectra of RuPc-BSA contained the absorption peaks of RuPc and BSA (Fig. 2 E). The above data proved that RuPc and BSA were successfully combined in this study to construct RuPc-BSA nanoparticles with excellent performance.

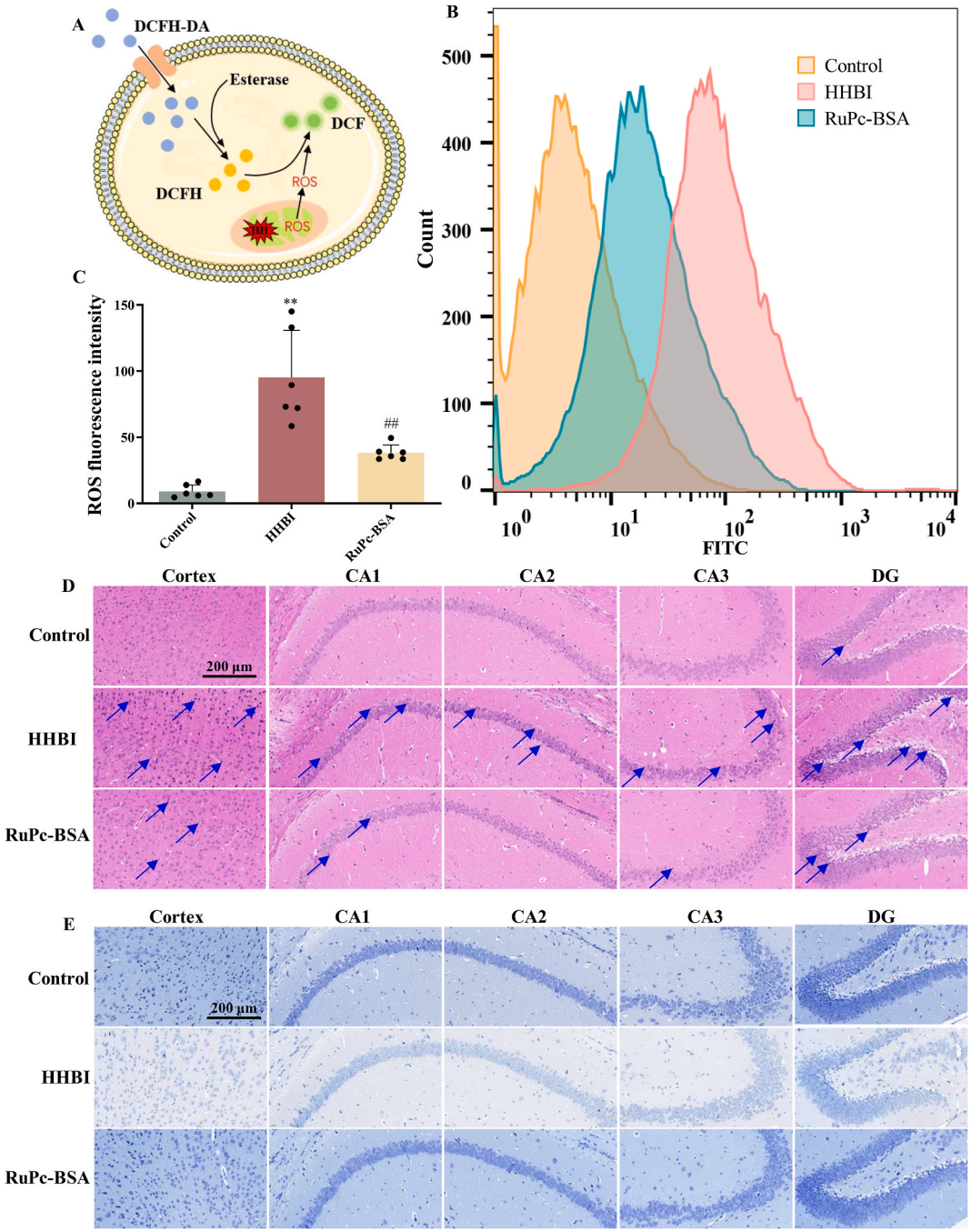

Fig. 4. RuPc-BSA alleviates neuronal damage by reducing ROS levels in the brain of HHBI mice. (A) The schematic scheme for determination of ROS. ROS signal intensity (B) and statistical results (C) of intracellular ROS content. H&E staining (D) and Nissl staining (E) of hippocampal CA1-CA3, DG and cortex (scale bar = 200 μm). Data above were presented as mean ± SD, n = 6. $^{**}p < 0.01$ vs the control group; $^{\#\#}p < 0.01$ vs the HHBI group.

3.2. Stability of RuPc-BSA

The stability of nanoprobe is an important factor affecting its therapeutic effect. Nanoprobes with insufficient stability may aggregate, disintegrate, or be broken down by various enzymes in the organism before reaching the target, greatly reducing the efficiency and accuracy of their diagnosis or treatment. As shown in Fig. 2 F, we analyzed the structural stability of RuPc-BSA nanoprobe in different media. The particle size change of RuPc-BSA in water, PBS, H_2O_2 and complete medium for 5 consecutive days was negligible, indicating that the RuPc-BSA structure had high stability.

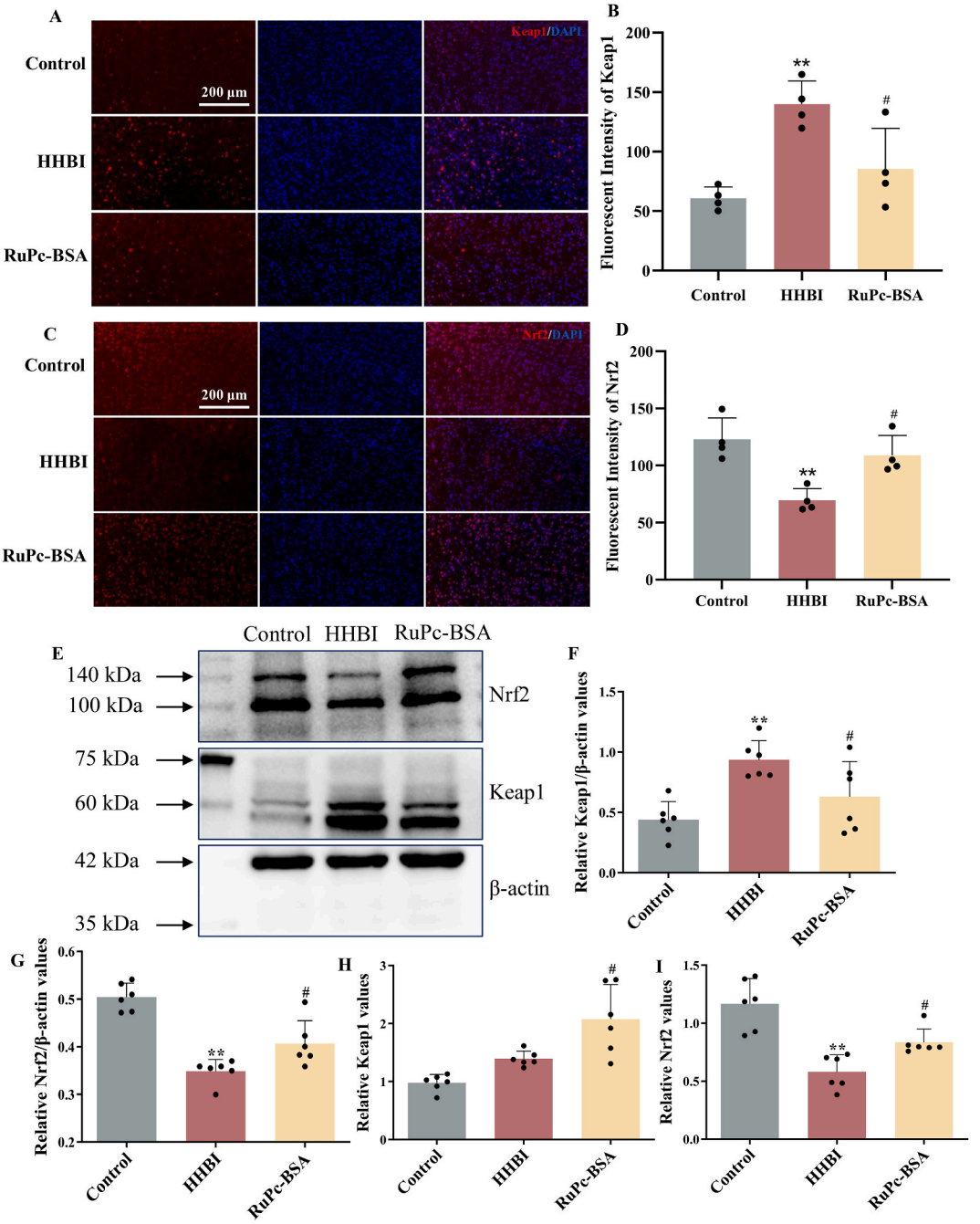

Fig. 5. RuPc-BSA promotes the expression of antioxidant factors by activating Keap1/Nrf2 signaling pathway. Fluorescence images (A) and statistical results (B) of Keap1. Fluorescence images (C) and statistical results (D) of Nrf2, n = 4. Western blotting analysis of Nrf2 and Keap1 proteins (E), and the statistical results of Keap1 (F) and Nrf2 (G). Keap1 (H) and Nrf2 (I) gene expression detection by qRT-PCR, n = 6. **p < 0.01 vs the control group; #p < 0.05 vs the HHBI group.

3.3. ROS scavenging potential of RuPc-BSA in vitro

The HHBI therapeutic effect of RuPc-BSA nanoprobe is reflected in the excellent ROS clearance effect. In this work, we *in vitro* examined the scavenging activity of various concentrations of RuPc-BSA on different types of ROS. As shown in Fig. 2G–I, RuPc-BSA showed significant scavenging effects on $HO^{\bullet}$, H_2O_2 and O_2^- in a dose-dependent manner. Specifically, the elimination impact of O_2^- was enhanced with increasing RuPc-BSA concentration. The above data prove that RuPc-BSA, as a probe with ROS scavenging ability, will be very promising for combating HHBI.

3.4. RuPc-BSA alleviates oxidative stress damage induced by HHBI

Modern studies have shown that a large amount of ROS accumulation in the state of ischemia and hypoxia will quickly overwhelm the antioxidant defense and lead to brain damage. In this paper, the levels of LDH (Fig. 3 A, $^{**}p < 0.01$) and MDA (Fig. 3 B, $^{**}p < 0.01$) in serum and brain tissue (LDH, Fig. 3C, $^{**}p < 0.01$; MDA, Fig. 3 D, $^{**}p < 0.01$) of HHBI group were memorably increased, while SOD (Serum, Fig. 3 E, $^{**}p < 0.01$; Brain tissue, Fig. 3 F, $^{**}p < 0.01$), CAT (Serum, Fig. 3 G, $^{**}p < 0.01$; Brain tissue, Fig. 3H, $^{**}p < 0.01$), GSSG (Serum, Fig. 3 I, $^{**}p < 0.01$; Brain tissue, Fig. 3 J) and GSH-PX (Serum, Fig. 3 K, $^{**}p < 0.01$; Brain tissue, Fig. 3 L, $^{**}p < 0.01$) were dramatically decreased compared with the control group. Surprisingly, the RuPc-BSA group signally reversed these abnormal indicators, indicating superior antioxidant activity. Furthermore, flow cytometry was used to identify the ROS fluorescence signals of cells in various treatment groups following the incubation of isolated HHBI mouse brain cells with DCFH-DA probes (Fig. 4 A). The results demonstrated that ROS content in the brain of mice in HHBI group was notably higher than that in control group (Fig. 4B and C, $^{**}p < 0.01$), and this phenomenon was prominently alleviated in RuPc-BSA group (Fig. 4B and C, $^{\#\#}p < 0.01$). Therefore, RuPc-BSA has eminent ability to erase ROS *in vivo* and reduce oxidative stress damage of HHBI mice.

3.5. RuPc-BSA alleviates brain pathological damage of HHBI mice

H&E and Nissl staining was employed to observe the effect of RuPc-BSA on general histopathological changes and neuronal activity in HHBI mice brains. H&E staining manifested that the neurons in the cerebral cortex and hippocampus of the control group were abundant and arranged regularly, and there was no obvious morphological and structural damage and capillary hyperemia and dilation. Compared with the control group, HHBI mice had apparent neuron loss, cell swelling, widening of the pericellular space, neuronal atrophy, nucleopytosis with dark staining, blood vessel dilation and congestion. After RuPc-BSA pre-administration, the characteristics of brain pathological injury in HHBI exposed mice were overtly mitigated (Fig. 4 D). The results of Nissl staining suggested that in the control group, the neural nuclear membrane and nucleolus were clearly defined and covered with abundant blue granular Nissl bodies. While the morphology of neurons in HHBI group was irregular, the Nissl staining was shallow, and the cell vitality was immensely decreased. Surprisingly, RuPc-BSA can tremendously reverse these pathological changes and enhance neuronal activity (Fig. 4 E).

3.6. RuPc-BSA activates Keap1/Nrf2 signaling pathway

In order to elucidate the molecular mechanism of the antioxidant effect of RuPc-BSA, we detected the effects of nanoprobe RuPc-BSA on the expression levels of Keap1/Nrf2 -related proteins and mRNA in the anti-oxidative stress pathway. As the main factor inducing HHBI, the oxidative stress balance of the body is usually rapidly broken under the stimulation of hypobaric hypoxia, which is manifested as the disturbance of Nrf2 ubiquitination. Immunofluorescence staining results showed that the HHBI mice had up-regulated Keap1 (Fig. 5A and B, $^{**}p < 0.01$) and down-regulated Nrf2 (Fig. 5C and D, $^{**}p < 0.01$) proteins expression, while the RuPc-BSA pre-administration stimulated Nrf2 protein level and restricted Keap1 protein level, suggesting that Keap1/Nrf2 antioxidant stress signaling pathway may be activated. Conformably, the results of Western blot further verified our hypothesis that RuPc-BSA intervention triggered Keap1/Nrf2 signaling pathway (Fig. 5 E and Multimedia component 1). Compared with the control group, the HHBI mice had up-regulated and down-regulated protein expression levels of Keap1 (Fig. 5E and F, $^{**}p < 0.01$) and Nrf2 (Fig. 5 E and G, $^{**}p < 0.01$), respectively, while the RuPc-BSA group had the exact opposite. In addition, mRNA levels of Nrf2 and Keap1 were also measured. Compared with the HHBI group, RuPc-BSA treatment increased Nrf2 mRNA levels, but Keap1 mRNA levels did not decrease as expected (Fig. 5H and I, $^{**}p < 0.01$, $^{\#}p < 0.05$).

3.7. Biosafety of RuPc-BSA

Safety evaluation is an indispensable step in the design and application of nanoprobes. The toxicity evaluation and structural modification of the probe can make it exert a therapeutic role while minimize its side effects on the organism. As shown in Fig. 6A and B, this study first evaluated the hemolysis effects of different concentrations of RuPc-BSA solutions. Compared with the control group, RuPc-BSA solution with a concentration of 10–100 μg/mL showed a slight hemolysis phenomenon, and the hemolysis rate of 100 μg/mL RuPc-BSA was only 6.73 ± 0.09 %, which did not exclude the interference of the color of the probe. Subsequently, H&E staining was used to analyze and evaluate the potential toxicity of RuPc-BSA in the heart, liver, spleen, lung, kidney and brain tissues of mice, and the results showed no obvious tissue lesions and cytotoxicity (Fig. 6C). Finally, we analyzed and detected the changes of blood index coefficient of RuPc-BSA pre-administrated mice. As shown in Fig. 6D–K, compared with the control group, the trend of changes in various blood indexes of mice in RuPc-BSA group remained at a small change range, and its specific parameters were basically

floating within the safe range. As a consequence, it is reasonable to conclude that the nanoprobe RuPc-BSA has a negligible toxicity and can be further employed as a ROS scavenger to prevent and treat HHBI.

4. Discussion

People who travel over 3000 m onto the plateau region have substantial brain damage due to increased formation of ROS in hypobaric and hypoxic conditions [35]. Individuals will experience and suffer AMS, chronic mountain sickness, and deadly brain edema if they do not adjust to and adapt to hypobaric and hypoxic insult [36,37]. Up to 80 % of visitors to the plateau region reportedly suffer from symptoms like headaches, sleeplessness, and disorientation [38]. Research has indicated that exposure to HH can cause oxidative stress damage as well as neuronal morphological alterations in the brain's cortex and hippocampal regions [39,40]. A number of issues, including elevated red blood cells, pulmonary hypertension, and reduced oxygen uptake and transport ability, can also result from prolonged exposure to an HH environment [41]. The intricacy of their targets has become a bottleneck in the development of new drugs, despite the fact that our earlier research revealed that the Tibetan medicine *Rhodiola crenulate* and its active component salidroside have excellent anti-ischemic stroke and anti-HHBI properties [42,43]. Encouragingly, large amounts of studies have declared that exogenous CO injection can reduce ROS generation, and the creation of CO nanoprobes with ROS-targeted clearance capabilities may provide a novel treatment strategy for HHBI [44,45].

CO can compete with oxygen and bind specifically to hemoglobin, which can disrupt blood oxygen transport and cause anoxic toxicity [46]. For a long time, CO was defined as a harmful substance to human body, until it was discovered that CO can also be produced by the heme oxygenase (HO) enzyme system. Numerous studies have demonstrated that the induced isoenzyme HO-1, which is the dominant phenotype of the HO enzyme, can interrupt oxidative stress signal transduction and aggravate hypoxic tissue damage [47,48]. Subsequently, the endogenous production of CO binds to the respiratory mitochondrial cytochrome heme group or NADPH

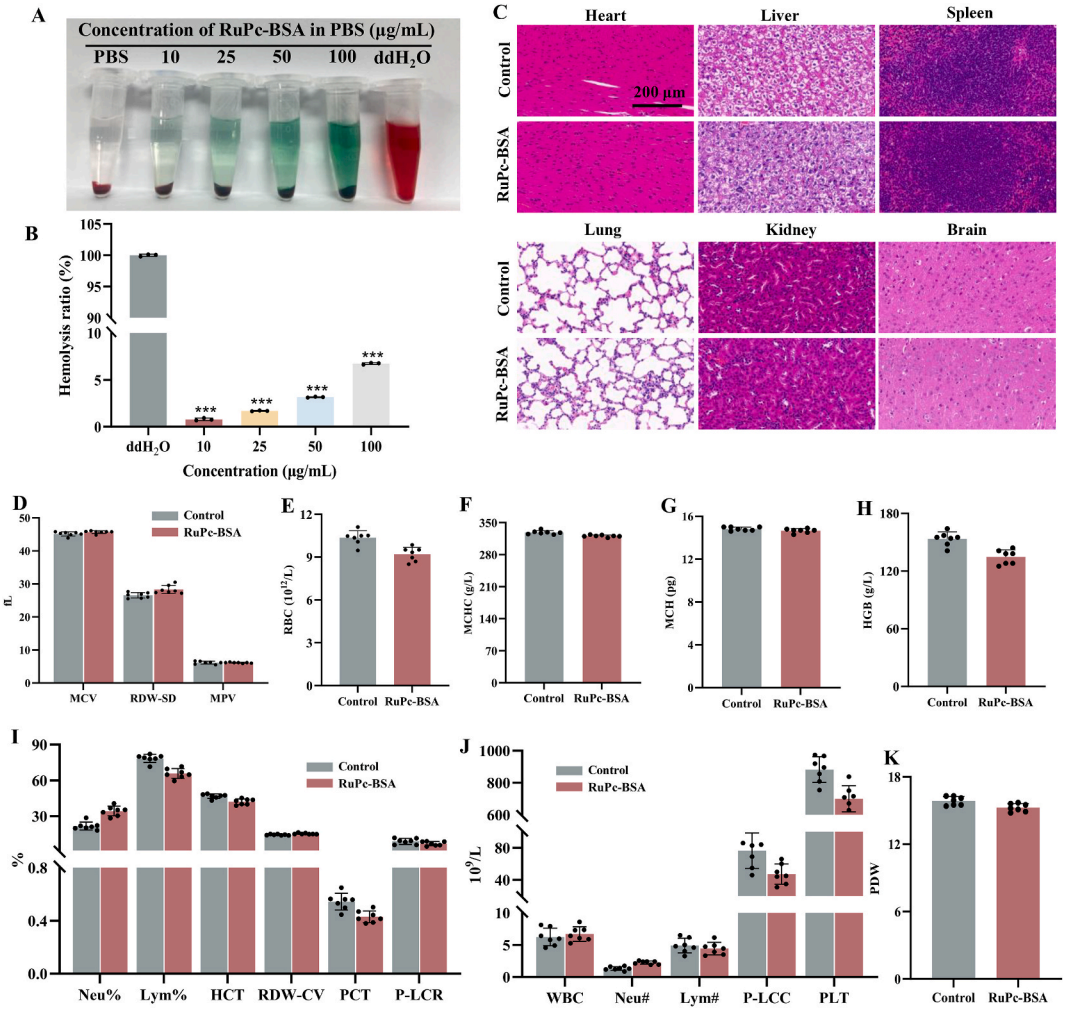

Fig. 6. Biosafety evaluation of RuPc-BSA nanoprobe. (A and B) Hemolysis rate of RuPc-BSA with different concentration. (C) The potential toxicity and side effects of RuPc-BSA in mice were evaluated by H&E staining. (D–K) Blood routine parameters of RuPc-BSA pretreated mice, n = 7.

oxidase, impeding brain damage by controlling the source of ROS production [49]. It was interesting to note that exogenous CO was found to produce the same therapeutic effect as endogenous CO due to the shared target of action [22]. In order to deliver CO to the wounded site while avoiding its hazardous side effects on the body, the limited water solubility of CO must be considered and overcome first. RuPc is a pharmacological CO donor with CORMS structure and has extraordinary potential for targeted CO delivery [29,50,51]. On this basis, RuPc was loaded onto BSA by self-assembly technology, and RuPc-BSA with higher water solubility and biosecurity was successfully constructed. Prior investigations have demonstrated that hypoxic situations can result in the BBB's integrity being destroyed, and that an imbalance in endothelial tight connections can cause a considerably vascular contents being entering into the brain [9,43]. As a spherical nanoparticle with an average particle size of 133 nm, the smaller volume makes RuPc-BSA more likely to enter into the brain parenchyma with the damage of BBB to play a pharmacological effect. The zeta potential of RuPc-BSA is −16.5 mV, making it show higher biocompatibility, while avoiding the disadvantages of positive charged nanoparticles that are easy to cause cytotoxicity and immunological reactions [52]. Polydispersion coefficient and SEM pictures further demonstrate RuPc-BSA's ability to be uniformly distributed in water. RuPc-BSA can also withstand long periods of stability in complete medium, PBS and water, with its particle size almost unchanged after five days. The stable structure of RuPc-BSA allows it to transport CO to the region of brain injury and target ROS clearing.

ROS is a general term for a class of oxygen-containing and active aerobic metabolites produced by the body, including O_2^-, H_2O_2, $HO^\bullet$ and singlet oxygen ($1O_2$) [53]. Under normal circumstances, ROS is crucial for preserving the internal environment's homeostasis and engaged in low-level intracellular signal transmission and regulation [54]. ROS levels increased significantly under HH exposure, and the imbalance between ROS and antioxidant system eventually led to oxidative stress damage. As shown in Fig. 2G–I, it was found that RuPc-BSA had splendid scavenging ability on O_2^-, H_2O_2 and $HO^\bullet$, among which O_2^- and $HO^\bullet$ had the best scavenging effect in a dose-dependent manner. Motivated by RuPc-BSA's excellent stability and *in vitro* ROS clearance effectiveness, we further assess RuPc-BSA's capacity to clear ROS *in vivo* and its potential to treat HHBI [32]. The pathological results showed that the space around the blood vessels in the hippocampus and cortical regions of the mouse brain tissue increased after HH exposure, the neurons shrank, and the nuclei shrank and showed dark staining. It's interesting to note that pre-treatment Balb/c mice with RuPc-BSA significantly reduced vascular edema and boosted neuronal activity, indicating alleviation from brain pathological injury. Numerous published studies have demonstrated that intracellular antioxidant enzymes, including SOD, GSH-Px and CAT, are capable of eliminating excess ROS generation quickly to prevent excessive ROS from damaging and overwhelming the antioxidant enzyme system. According to our research, HHBI raised the amounts of LDH, MDA, and other toxic compounds while decreasing the levels of SOD, CAT, GSSG, and GSH-px in serum and brain tissue. However, RuPc-BSA corrected these abnormally expressed markers of oxidative stress in the serum and hippocampal tissues of HHBI mice. Results from flow cytometry demonstrated a considerable reduction in ROS levels in the brains of HHBI mice treated with RuPc-BSA, which was highly compatible with our anticipated outcomes. It is worth noting that the antioxidant function of RuPc-BSA may also have a synergistic effect on the regulation of Keap1/Nrf2 redox signaling [55–57]. It has been confirmed that exposure to high levels of ROS can trigger the Keap1/Nrf2 signaling pathway, hence facilitating the separation of Nrf2 and Keap1 [58,59]. Subsequently, the Nrf2 transcription factor activates the transcription of some cell protection genes, such as CAT and SOD [60,61]. Our results revealed that RuPc-BSA treatment reduced Keap1 expression and increased Nrf2 expression.

5. Conclusions

In this study, we developed a novel RuPc-BSA nanoparticle with ROS-targeted clearance function to treat HHBI. RuPc-BSA is a CO delivery system with CORMS structure, which reduces ROS production by delivering CO to damaged mitochondria. *In vitro* experiments attested that RuPc-BSA has higher stability and biosafety with a noteworthy scavenging potential for ROS. In HHBI mice with RuPc-BSA pre-administration, oxidative stress damage in mice brain was memorably reduced, and brain neuron activity was observably increased. The antioxidant capacity of RuPc-BSA maybe related to the activation of the Keap1/Nrf2 signaling pathway.

Data availability statement

The authors confirm that the data supporting the findings of this study are available within the article.

Ethics declarations

The operations and procedures involved in animal experiments were reviewed and approved by the Animal Research Ethics Committee of Chengdu University of Traditional Chinese Medicine (Approval number: 2022–83).

CRediT authorship contribution statement

Xiaobo Wang: Conceptualization. **Fuhan Fan:** Writing – original draft, Validation. **Ya Hou:** Validation, Data curation. **Xianli Meng:** Writing – review & editing.

Declaration of competing interest

The authors declare the following financial interests/personal relationships which may be considered as potential competing interests:Xiaobo Wang reports financial support was provided by National Natural Science Foundation of China. If there are other

authors, they declare that they have no known competing financial interests or personal relationships that could have appeared to influence the work reported in this paper.

Acknowledgements

We appreciate the financial support from the National Natural Science Foundation of China (82104533 and 82274207), the Science Foundation for Youths of Science & Technology Department of Sichuan Province (2024NSFSC1845 and 2023NSFSC1776) and Xinglin Scholar Research Promotion Project of Chengdu University of TCM (XKTD2022013). The authors would like to thank Zhiguo Zhou, a research scholar in the College of Chemistry and Materials Science, Shanghai Normal University, for providing RuPc-BSA nanoprobe.

Appendix A. Supplementary data

Supplementary data to this article can be found online at https://doi.org/10.1016/j.heliyon.2024.e38958.

References

[1] A. Boucly, J. Weatherald, L. Savale, X. Jaïs, V. Cottin, G. Prevot, F. Picard, P. de Groote, M. Jevnikar, E. Bergot, A. Chaouat, C. Chabanne, A. Bourdin, F. Parent, D. Montani, G. Simonneau, M. Humbert, O. Sitbon, Risk assessment, prognosis and guideline implementation in pulmonary arterial hypertension, Eur. Respir. J. 50 (2) (2017 Aug) 1700889, https://doi.org/10.1183/13993003.00889-2017.

[2] J.B. West, Oxygen Conditioning: a new technique for improving living and working at high altitude, Physiology 31 (3) (2016 May) 216–222, https://doi.org/10.1152/physiol.00057.2015.

[3] Y. Xue, X. Wang, B. Wan, D. Wang, M. Li, K. Cheng, Q. Luo, D. Wang, Y. Lu, L. Zhu, Caveolin-1 accelerates hypoxia-induced endothelial dysfunction in high-altitude cerebral edema, Cell Commun. Signal. 20 (1) (2022 Oct) 160, https://doi.org/10.1186/s12964-022-00976-3.

[4] L. Taylor, S.L. Watkins, H. Marshall, B.J. Dascombe, J. Foster, The impact of different environmental conditions on cognitive function: a focused review, Front. Physiol. 6 (2016 Jan) 372, https://doi.org/10.3389/fphys.2015.00372.

[5] A.M. Luks, E.R. Swenson, P. Bärtsch, Acute high-altitude sickness, Eur. Respir. Rev. 26 (143) (2017 Jan) 160096, https://doi.org/10.1183/16000617.0096-2016.

[6] X. Wang, G. Chen, B. Wan, Z. Dong, Y. Xue, Q. Luo, D. Wang, Y. Lu, L. Zhu, NRF1-mediated microglial activation triggers high-altitude cerebral edema, J. Mol. Cell Biol. 14 (5) (2022 Sep) mjac036, https://doi.org/10.1093/jmcb/mjac036.

[7] S. Riech, K. Kallenberg, O. Moerer, P. Hellen, P. Bärtsch, M. Quintel, M. Knauth, The pattern of brain microhemorrhages after severe lung failure resembles the one seen in high-altitude cerebral edema, Crit. Care Med. 43 (9) (2015 Sep) e386–e389, https://doi.org/10.1097/CCM.0000000000001150.

[8] C. Wang, M. Yan, H. Jiang, Q. Wang, S. He, J. Chen, C. Wang, Mechanism of aquaporin 4 (AQP 4) up-regulation in rat cerebral edema under hypobaric hypoxia and the preventative effect of puerarin, Life Sci. 193 (2018 Jan) 270–281, https://doi.org/10.1016/j.lfs.2017.10.021.

[9] S. Jiang, F. Fan, L. Yang, K. Chen, Z. Sun, Y. Zhang, N. Cairang, X. Wang, X. Meng, Salidroside attenuates high altitude hypobaric hypoxia-induced brain injury in mice via inhibiting NF-κB/NLRP3 pathway, Eur. J. Pharmacol. 925 (2022 Jun) 175015, https://doi.org/10.1016/j.ejphar.2022.175015.

[10] Y. Tang, Y. Hou, Y. Zeng, Y. Hu, Y. Zhang, X. Wang, X. Meng, Salidroside attenuates $CoCl_2$-simulated hypoxia injury in PC12 cells partly by mitochondrial protection, Eur. J. Pharmacol. 912 (2021 Dec) 174617, https://doi.org/10.1016/j.ejphar.2021.174617.

[11] D. Coimbra-Costa, N. Alva, M. Duran, T. Carbonell, R. Rama, Oxidative stress and apoptosis after acute respiratory hypoxia and reoxygenation in rat brain, Redox Biol. 12 (2017 Aug) 216–225, https://doi.org/10.1016/j.redox.2017.02.014.

[12] M. Zhao, P. Zhu, M. Fujino, J. Zhuang, H. Guo, I. Sheikh, L. Zhao, X.K. Li, Oxidative stress in hypoxic-ischemic encephalopathy: molecular mechanisms and therapeutic strategies, Int. J. Mol. Sci. 17 (12) (2016) 2078, https://doi.org/10.3390/ijms17122078.

[13] A. Frati, D. Cerretani, A.I. Fiaschi, P. Frati, V. Gatto, R. La Russa, A. Pesce, E. Pinchi, A. Santurro, F. Fraschetti, V. Fineschi, Diffuse axonal injury and oxidative stress: a comprehensive review, Int. J. Mol. 18 (12) (2017 Dec) 2600, https://doi.org/10.3390/ijms18122600.

[14] L. Barna, F.R. Walter, A. Harazin, A. Bocsik, A. Kincses, V. Tubak, K. Jósvay, Á. Zvara, P. Campos-Bedolla, M.A. Deli, Simvastatin, edaravone and dexamethasone protect against kainate-induced brain endothelial cell damage, Fluids, Barriers. CNS. 17 (1) (2020 Feb) 5, https://doi.org/10.1186/s12987-019-0166-1.

[15] N. Xie, F. Fan, S. Jiang, Y. Hou, Y. Zhang, N. Cairang, X. Wang, X. Meng, *Rhodiola crenulate* alleviates hypobaric hypoxia-induced brain injury via adjusting NF-κB/NLRP3-mediated inflammation, Phytomedicine 103 (2022 Aug) 154240, https://doi.org/10.1016/j.phymed.2022.154240.

[16] D. Sacks, B. Baxter, B.C.V. Campbell, J.S. Carpenter, C. Cognard, D. Dippel, M. Eesa, U. Fischer, K. Hausegger, J.A. Hirsch, M. Shazam Hussain, O. Jansen, M. V. Jayaraman, A.A. Khalessi, B.W. Kluck, S. Lavine, P.M. Meyers, S. Ramee, D.A. Rüfenacht, C.M. Schirmer, D. Vorwerk, Multisociety consensus quality improvement revised consensus statement for endovascular therapy of acute ischemic stroke, Int. J. Stroke 13 (6) (2018 Aug) 612–632, https://doi.org/10.1177/1747493018778713.

[17] C. Winter, T. Bjorkman, S. Miller, P. Nichols, J. Cardinal, P. O'Rourke, E. Ballard, F. Nasrallah, V. Vegh, Acute mountain sickness following incremental trekking to high altitude: correlation with plasma vascular endothelial growth factor levels and the possible effects of dexamethasone and acclimatization following re-exposure, Front. Physiol. 12 (2021 Oct) 746044, https://doi.org/10.3389/fphys.2021.746044.

[18] T.T. Tien Vo, Q.C. Vo, V.P. Tuan, Y. Wee, H.C. Cheng, I.T. Lee, The potentials of carbon monoxide-releasing molecules in cancer treatment: an outlook from ROS biology and medicine, Redox. Biol. Redox. Biol. 46 (2021 Oct) 102124, https://doi.org/10.1016/j.redox.2021.102124.

[19] C. Mattiuzzi, G. Lippi, Worldwide epidemiology of carbon monoxide poisoning, Hum. Exp. Toxicol. 39 (4) (2020 Apr) 387–392, https://doi.org/10.1177/0960327119891214.

[20] B. Chance, G.R. Williams, The respiratory chain and oxidative phosphorylation, Adv. Enzymol. Relat. Subj. Biochem. 17 (1956) 65–134, https://doi.org/10.1002/9780470122624.ch2.

[21] D.R. Hess, Inhaled carbon monoxide: from toxin to therapy, Respir. Care 62 (10) (2017 Oct) 1333–1342, https://doi.org/10.4187/respcare.05781.

[22] R. Motterlini, R. Foresti, Biological signaling by carbon monoxide and carbon monoxide-releasing molecules, Am. J. Physiol. Cell. Physiol. 312 (3) (2017 Mar) C302–C313, https://doi.org/10.1152/ajpcell.00360.2016.

[23] D.C. Fuhrmann, B. Brüne, Mitochondrial composition and function under the control of hypoxia, Redox Biol. 12 (2017 Aug) 208–215, https://doi.org/10.1016/j.redox.2017.02.012.

[24] J.A. Willson, S. Arienti, P. Sadiku, L. Reyes, P. Coelho, T. Morrison, G. Rinaldi, D.H. Dockrell, M.K.B. Whyte, S.R. Walmsley, Neutrophil HIF-1α stabilization is augmented by mitochondrial ROS produced via the glycerol 3-phosphate shuttle, Blood 139 (2) (2022 Jan) 281–286, https://doi.org/10.1182/blood.2021011010.

[25] S.S. Jung, J.S. Moon, J.F. Xu, E. Ifedigbo, S.W. Ryter, A.M. Choi, K. Nakahira, Carbon monoxide negatively regulates NLRP3 inflammasome activation in macrophages, Am. J. Physiol. Lung Cell Mol. Physiol. 308 (10) (2015 May) L1058–L1067, https://doi.org/10.1152/ajplung.00400.2014.

[26] S.W. Ryter, K.C. Ma, A.M.K. Choi, Carbon monoxide in lung cell physiology and disease, Am. J. Physiol. Cell. Physiol 314 (2) (2018 Feb) C211–C227, https://doi.org/10.1152/ajpcell.00022.2017.

[27] U. Goebel, J. Wollborn, Carbon monoxide in intensive care medicine-time to start the therapeutic application? Intensive. Care. Med. Exp. 8 (1) (2020 Jan) 2, https://doi.org/10.1186/s40635-020-0292-8.

[28] R. Motterlini, J.E. Clark, R. Foresti, P. Sarathchandra, B.E. Mann, C.J. Green, Carbon monoxide-releasing molecules: characterization of biochemical and vascular activities, Circ. Res. 90 (2) (2002 Feb) E17–E24, https://doi.org/10.1161/hh0202.104530.

[29] A.P. Kroitor, L.P. Cailler, A.G. Martynov, Y.G. Gorbunova, A.Y. Tsivadze, A.B. Sorokin, Unexpected formation of a μ-carbido diruthenium (iv) complex during the metalation of phthalocyanine with $Ru_3(CO)_{12}$ and its catalytic activity in carbene transfer reactions, Dalton Trans. (45) (2017) 15651–15655, https://doi.org/10.1039/c7dt03703a, 2017 Nov.

[30] C.Y. Hsu, T.T.T. Vo, C.W. Lee, Y.L. Chen, W.N. Lin, H.C. Cheng, Q.C. Vo, I.T. Lee, Carbon monoxide releasing molecule-2 attenuates angiotensin II-induced IL-6/Jak2/Stat3-associated inflammation by inhibiting NADPH oxidase- and mitochondria-derived ROS in human aortic smooth muscle cells, Biochem. Pharmacol. 198 (2022 Apr) 114978, https://doi.org/10.1016/j.bcp.2022.114978.

[31] N. Li, Q. Li, J. Bai, K. Chen, H. Yang, W. Wang, F. Fan, Y. Zhang, X. Meng, T. Kuang, G. Fan, The multiple organs insult and compensation mechanism in mice exposed to hypobaric hypoxia, Cell. Stress. Chaperones. 25 (5) (2020 Sep) 779–791, https://doi.org/10.1007/s12192-020-01117-w.

[32] K. Chen, N. Li, F. Fan, Z. Geng, K. Zhao, J. Wang, Y. Zhang, C. Tang, X. Wang, X. Meng, Tibetan medicine Duoxuekang Capsule ameliorates high-altitude polycythemia accompanied by brain injury, Front. Pharmacol. 12 (2021 May) 680636, https://doi.org/10.3389/fphar.2021.680636.

[33] L. Yang, Y. Tao, L. Luo, Y. Zhang, X. Wang, X. Meng, Dengzhan Xixin injection derived from a traditional Chinese herb *Erigeron breviscapus* ameliorates cerebral ischemia/reperfusion injury in rats via modulation of mitophagy and mitochondrial apoptosis, J. Ethnopharmacol. 288 (2022 Apr) 114988, https://doi.org/10.1016/j.jep.2022.

[34] X. Wang, Y. Tang, N. Xie, J. Bai, S. Jiang, Y. Zhang, Y. Hou, X. Meng, Salidroside, a phenyl ethanol glycoside from *Rhodiola crenulata*, orchestrates hypoxic mitochondrial dynamics homeostasis by stimulating Sirt1/p53/Drp1 signaling, J. Ethnopharmacol. 293 (2022 Jul) 115278, https://doi.org/10.1016/j.jep.2022.115278.

[35] J. Ma, C. Wang, Y. Sun, L. Pang, S. Zhu, Y. Liu, L. Zhu, S. Zhang, L. Wang, L. Du, Comparative study of oral and intranasal puerarin for prevention of brain injury induced by acute high-altitude hypoxia, Int. J. Pharm. 591 (2020 Dec) 120002, https://doi.org/10.1016/j.ijpharm.2020.120002.

[36] Y. Li, Y. Zhang, Y. Zhang, Research advances in pathogenesis and prophylactic measures of acute high altitude illness, Respir. Med. 145 (2018 Dec) 145–152, https://doi.org/10.1016/j.rmed.2018.11.004.

[37] B. Coustet, F.J. Lhuissier, R. Vincent, J.P. Richalet, Electrocardiographic changes during exercise in acute hypoxia and susceptibility to severe high-altitude illnesses, Circulation 131 (9) (2015 Mar) 786–794, https://doi.org/10.1161/CIRCULATIONAHA.

[38] N. Netzer, K. Strohl, M. Faulhaber, H. Gatterer, M. Burtscher, Hypoxia-related altitude illnesses, J. Travel. Med. 20 (4) (2013 Jul) 247–255, https://doi.org/10.1111/jtm.12017.

[39] M. Li, Y. Zhu, J. Li, L. Chen, W. Tao, X. Li, Y. Qiu, Effect and mechanism of verbascoside on hypoxic memory injury in plateau, Phytother Res. 33 (10) (2019 Oct) 2692–2701, https://doi.org/10.1002/ptr.6443.

[40] J. Shi, J. Wang, J. Zhang, X. Li, X. Tian, W. Wang, P. Wang, M. Li, Polysaccharide extracted from *Potentilla anserina* L ameliorate acute hypobaric hypoxia-induced brain impairment in rats, Phytother Res. 34 (9) (2020 Sep) 2397–2407, https://doi.org/10.1002/ptr.6691.

[41] M. Lu, N. Tsring, T. Yu, J. Wu, S. Wong, G. Chen, P. Dekyi, F. Pan, S. Xian, D. Rinchen, Y. Mao, L. Zhang, B. Yao, Protective effects of traditional Tibetan medicine Zuo-Mu-A Decoction on the blood parameters and myocardium of high altitude polycythemia model rats, Chin. J. Integr. Med. 23 (12) (2017 Dec) 908–915, https://doi.org/10.1007/s11655-016-2500-7.

[42] F. Fan, L. Yang, R. Li, X. Zou, N. Li, X. Meng, Y. Zhang, X. Wang, Salidroside as a potential neuroprotective agent for ischemic stroke: a review of sources, pharmacokinetics, mechanism and safety, Biomed. Pharmacother. 129 (2020 Sep) 110458, https://doi.org/10.1016/j.biopha.2020.110458.

[43] F. Fan, H. Jiang, Y. Hou, Y. Zhang, Q. Zhao, Y. Zeng, X. Meng, X. Wang, Barrier functional integrity recording on bEnd.3 vascular endothelial cells via transendothelial electrical resistance detection, J. Vis. Exp. 199 (2023 Sep), https://doi.org/10.3791/65938.

[44] Y.K. Choi, J.H. Kim, D.K. Lee, K.S. Lee, M.H. Won, D. Jeoung, H. Lee, K.S. Ha, Y.G. Kwon, Y.M. Kim, Carbon monoxide potentiation of L-type Ca^{2+} channel activity increases HIF-1α-independent VEGF expression via an AMPKα/SIRT1-mediated PGC-1α/ERRα axis, Antioxid. Redox. Signal. 27 (1) (2017 Jul) 21–36, https://doi.org/10.1089/ars.2016.6684.

[45] Y.K. Choi, J.H. Park, J.A. Yun, J.H. Cha, Y. Kim, M.H. Won, K.W. Kim, K.S. Ha, Y.G. Kwon, Y.M. Kim, Heme oxygenase metabolites improve astrocytic mitochondrial function via a Ca^{2+}-dependent HIF-1α/ERRα circuit, PLoS One 13 (8) (2018 Aug) e0202039, https://doi.org/10.1371/journal.pone.0202039.

[46] S.W. Ryter, L.E. Otterbein, Carbon monoxide in biology and medicine, Bioessays 26 (3) (2004 Mar) 270–280, https://doi.org/10.1002/bies.20005.

[47] S.W. Ryter, A.M. Choi, Carbon monoxide: present and future indications for a medical gas, Korean, J. Intern. 28 (2) (2013 Mar) 123–140, https://doi.org/10.3904/kjim.2013.28.2.123.

[48] K.A. Nath, Heme oxygenase-1: a provenance for cytoprotective pathways in the kidney and other tissues, Kidney, Int 70 (3) (2006 Aug) 432–443, https://doi.org/10.1038/sj.ki.5001565.

[49] C. Taillé, J. El-Benna, S. Lanone, J. Boczkowski, R. Motterlini, Mitochondrial respiratory chain and NAD(P)H oxidase are targets for the antiproliferative effect of carbon monoxide in human airway smooth muscle, J. Biol. Chem. 280 (27) (2005 Jul) 25350–25360, https://doi.org/10.1074/jbc.M503512200.

[50] G.Y. Lee, A. Zeb, E.H. Kim, B. Suh, Y.J. Shin, D. Kim, K.W. Kim, Y.H. Choe, H.I. Choi, C.H. Lee, O.S. Qureshi, I.B. Han, S.Y. Chang, O.N. Bae, J.K. Kim, CORM-2-entrapped ultradeformable liposomes ameliorate acute skin inflammation in an ear edema model via effective CO delivery, Acta Pharm. Sin. B 10 (12) (2020 Dec) 2362–2373, https://doi.org/10.1016/j.apsb.2020.05.010.

[51] Z. Yuan, X. Yang, B. Wang, Redox and catalase-like activities of four widely used carbon monoxide releasing molecules (CO-RMs), Chem. Sci. 12 (39) (2021 Sep) 13013–13020, https://doi.org/10.1039/d1sc03832j.

[52] L.W.C. Ho, Y. Liu, R. Han, Q. Bai, C.H.J. Choi, Nano-cell interactions of non-cationic bionanomaterials, Acc. Chem. Res. 52 (6) (2019 Jun) 1519–1530, https://doi.org/10.1021/acs.accounts.9b00103.

[53] T.P. Cash, Y. Pan, M.C. Simon, Reactive oxygen species and cellular oxygen sensing, Free Radic. Biol. Med. 43 (9) (2007 Nov) 1219–1225, https://doi.org/10.1016/j.freeradbiomed.2007.07.001.

[54] R. Liu, C. Xu, W. Zhang, Y. Cao, J. Ye, B. Li, S. Jia, L. Weng, Y. Liu, L. Liu, M. Zheng, FUNDC1-mediated mitophagy and HIF1α activation drives pulmonary hypertension during hypoxia, Cell Death Dis. 13 (7) (2022 Jul) 634, https://doi.org/10.1038/s41419-022-05091-2.

[55] P.L. Chi, C.C. Lin, Y.W. Chen, L.D. Hsiao, C.M. Yang, CO induces Nrf2-dependent heme oxygenase-1 transcription by cooperating with Sp1 and c-Jun in rat brain astrocytes, Mol. Neurobiol. 52 (1) (2015 Aug) 277–292, https://doi.org/10.1007/s12035-014-8869-4.

[56] C. Liu, M. Rokavec, Z. Huang, H. Hermeking, Curcumin activates a ROS/KEAP1/NRF2/miR-34a/b/c cascade to suppress colorectal cancer metastasis, Cell Death Differ. 30 (7) (2023 Jul) 1771–1785, https://doi.org/10.1038/s41418-023-01178-1.

[57] C. Lin, L.D. Hsiao, R.L. Cho, C. Yang, CO-releasing molecule-2 induces Nrf2/ARE-dependent heme oxygenase-1 expression suppressing TNF-α-induced pulmonary inflammation, J. Clin. Med. 8 (4) (2019 Mar) 436, https://doi.org/10.3390/jcm8040436.

[58] M. Kobayashi, M. Yamamoto, Molecular mechanisms activating the Nrf2-Keap1 pathway of antioxidant gene regulation, Antioxid. Redox. Signal. 7 (3) (2005 Mar) 385–394, https://doi.org/10.1089/ars.2005.7.385.

[59] T. Suzuki, M. Yamamoto, Molecular basis of the keap1-nrf2 system, free, Radic. Biol. Med. 88 (2015 Nov) 93–100, https://doi.org/10.1016/j.freeradbiomed.2015.06.006.

[60] R. Zhang, M. Xu, Y. Wang, F. Xie, G. Zhang, X. Qin, Nrf2-a promising therapeutic target for defensing against oxidative stress in stroke, Mol. Neurobiol. 54 (8) (2017 Oct) 6006–6017, https://doi.org/10.1007/s12035-016-0111-0.

[61] Y. Korenori, S. Tanigawa, T. Kumamoto, S. Qin, Y. Daikoku, K. Miyamori, M. Nagai, D. Hou, Modulation of Nrf2/Keap1 system by Wasabi 6-methylthiohexyl isothiocyanate in ARE-mediated NQO1 expression, Mol. Nutr. Food Res. 57 (5) (2013 May) 854–864, https://doi.org/10.1002/mnfr.201200689.